Analytical, Numerical 1D and 3D Water Hammer Investigations in a Simple Pipeline Apparatus

Anton Bergant[1,2] ✉ – Zlatko Rek[2] – Kamil Urbanowicz[3]

1 Litostroj Power d.o.o., Slovenia
2 University of Ljubljana, Faculty of Mechanical Engineering, Slovenia
3 West Pomeranian University of Technology in Szczecin, Faculty of Mechanical Engineering and Mechatronics, Poland

✉ anton.bergant@litostrojpower.eu

Abstract *This paper deals with the analytical and numerical simulation of a water hammer in the reservoir-pipeline-valve (RPV) system. An analytical solution of the water hammer equations with unsteady friction term was derived for transient laminar pipe flow in a RPV system. For simulation of an arbitrary flow situation a number of one-dimensional (1D) numerical methods have been developed. The physically based method of characteristics proved to be computationally efficient and can handle complex boundary conditions. The accuracy of the 1D numerical model is increased by introducing terms that take into account 3D effects (example of an unsteady skin friction). The 3D model predicts these influences directly and represents an excellent tool for researching multidimensional properties of fluids (numerical laboratory). Calculation results based on 1D and 3D numerical models are in good agreement with results of measurements taking into account adequate prediction and modelling of influential physical parameters during laminar and low-Reynolds number turbulent water hammer events. Quantitative comparison analysis yields up to 2 % difference in maximum head at the valve and up to 5 % relative difference in pressure head drop at the midpoint of the pipeline monitored over the first four positive pressure pulses.*

Keywords *pipeline, water hammer, analytical solution, method of characteristics, computational fluid dynamics, unsteady skin friction*

Highlights

- *Convolution-based unsteady friction model accurately captures water hammer wave mechanics.*
- *Analytical 1D laminar model effectively applies to low-Re number turbulent water hammer.*
- *Indirect 1D and direct 3D friction approaches yield similar responses to water hammer disturbances.*
- *1D and 3D models successfully validated against rapid water hammer experiments.*

1 INTRODUCTION

Hydraulic piping systems, such as those found in hydroelectric power plants, water supply networks, operate under different flow conditions. A change in flow rate causes a pressure rise and drop in the system. Hydraulic transients in piping systems (water hammer, hydraulic vibrations) can induce extreme pressures, formation of large local vapour cavities and distributed cavitating flow zones (zones of negative pressure), liquid and structural vibrations, and mass oscillations [1-3]. Transient loads are kept within the permissible limits by water hammer control means that include (i) alteration of operational regimes (valve closure time, limitation of hydraulic turbine maximum output, decrease of maximum flow rate), (ii) installation of surge control devices in the system (additional flywheel, air vessel, surge tank, pressure regulating valve, air valve) and (iii) redesign of the flow-passage system layout (pipeline diameter, pipe-wall material, change in elevation) [4-6]. In this paper, we investigate a water hammer, which is induced by an aperiodic change in the pipe flow velocity. The theoretical analysis of pressure changes in systems by solving the classic 1D water hammer equations gives reliable results as long as the conditions in the derivation of these equations are valid. In practice, the conditions in piping system may be far from the idealized situation described by the classic water hammer equations. For example, the steady skin friction model does not produce sufficient damping for rapid transient events [7,8]. Consequently, we use more advanced models of unsteady skin friction, which include the influence of two-dimensional (2D) and 3D effects [9-12].

In engineering practice, many other discrepancies can occur, such as: air (free and dissolved) in the liquid, transient cavitation, fluid-structure interaction (particularly if the pipes are not rigidly fixed or the excitation is severe), viscoelastic behavior of the pipe wall (in polymer pipes or if steel pipes deform plastically), as well as leaks and blockages in the pipeline [13]. In this paper, we will discuss the influence of unsteady skin friction indirectly with the help of a frozen-viscosity convolutional 1D model and directly with 3D numerical calculations [14]. It is desirable to solve 1D water hammer equations analytically. Unfortunately an exact solution for the water hammer equations with consideration of unsteady skin friction exists only for transient laminar pipe flow situation [15]. Therefore, a numerical 1D model is used in industry for treatment of both transient laminar and turbulent pipe flows. In our paper the numerical 1D model is based on the method of characteristics (MOC), which is most suitable for solving water hammer equations [1]. However, we will test the analytical solution for transient laminar pipe flow for low-Reynolds number transient turbulent flow situation. Computational fluid dynamics (CFD) is today, with increasingly powerful computers, a very useful tool in the analysis of transient flows and phenomena in hydraulic pipelines and devices [16,17]. So, for example, in [18], Saemi et al. studied the phenomenon of water hammer and analyzed the influence of the outlet boundary condition (flow reduction curves and valve modelling). They also analyzed the 3D effects caused by valve closure and the turbulence structure during the occurrence of water hammer. In [19], Cao et al. presented an alternative 3D CFD model for the systematic investigation of the dynamic characteristics of flow under transient conditions in a hydraulic pipe. The characteristics of the ball valve under static and

dynamic conditions were analyzed in detail and the effect of closing time on the head loss coefficient and the discharge coefficient was carefully investigated. In addition, coupled 1D and 3D method can be used for flow situations where 3D effects prevail in a small part of the hydraulic pipeline system [20].

The objective of this paper is to extend the application of the analytical model developed for laminar water hammer [15] to low-Reynolds number turbulent water hammer. The analytical model will be presented in a novel form with defined optimized upper limit of the nominally infinite sum in the solution. Similarly, the effectiveness of Zielke's weighting function [21] in 1D unsteady friction models will be validated for low-Reynolds number turbulent transient pipe flow. In our 3D investigations the CFD package ANSYS Fluent Release 18.2 [22] will be used. A particular emphasis will be given to selection of the most appropriate turbulence model for a turbulent water hammer. The presented 1D and 3D models will be validated against the results of measurements in a simple pipeline apparatus [8]. Theoretical and experimental investigations in this paper should deepen the understanding of water hammer phenomena in liquid-filled piping systems.

2 METHODS & MATERIALS

Water hammer describes the propagation of pressure waves in pipes with liquid. In most engineering applications the cross-sectional dimension of the pipe is negligible compared to the length of the pipe. Assuming uniform flow and neglecting small convective terms yields the following two 1D unsteady pipe flow equations, (i) the continuity equation and (ii) the equation of motion [1,2]

$$\frac{\partial H}{\partial t}+\frac{a^2}{gA}\frac{\partial Q}{\partial x}=0, \tag{1}$$

$$\frac{\partial H}{\partial x}+\frac{1}{gA}\frac{\partial Q}{\partial t}+f\frac{Q|Q|}{2gDA^2}=0, \tag{2}$$

in which H is piezometric head (head), t time, Q discharge, x distance along the pipe, a pressure wave speed, g gravitational acceleration, A pipe cross-sectional area, f Darcy-Weisbach friction factor and D inner pipe diameter. The symbols are explained as they first appear in the paper.

In Equation (2), we traditionally use the steady-state Darcy-Weisbach friction coefficient f. In the case of fast transient phenomena, the steady friction coefficient is modified by introducing a non-stationary friction term. The friction coefficient f is expressed as the sum of a steady (or quasi-steady) part f_q and the unsteady part f_u. In this paper, we will use the frozen- viscosity convolution-based unsteady friction model [21,23,24] in which the unsteady part is defined by the convolution of a weighting function W_0 with past temporal accelerations

$$f_u=\frac{32\nu A}{DQ|Q|}\int_0^t\frac{\partial Q}{\partial t^*}W_0\left(t-t^*\right)dt^*, \tag{3}$$

in which ν is kinematic viscosity and W_0 weighting function.

The unsteady part is a result of inverse Laplace transformation of the quasi-2D water hammer Laplacian-solution in the frequency domain. Weighting functions have been developed for transient laminar [21] and turbulent pipe flow [25,26]. The frozen-viscosity convolution-based unsteady friction model is suitable for water hammer flows where pressure waves travel at sound propagation speed and decelerate/accelerate the flow in short time periods [27]. The importance of unsteady friction in water hammer flows is decreased with increasing pre-transient Reynolds number [28].

The classical 1D water hammer equations will be solved by (i) the analytical method and (ii) the MOC. Finally, (iii) the 3D numerical solution of the Navier-Stokes equations will be presented and applied to water hammer problems.

2.1 Analytical Solution of Water Hammer Equations

Analytical solutions of water hammer Eqs. (1) and (2) for frictionless pipe systems and for systems with consideration of quasi-steady friction have been developed by Rich in the middle of the previous century [29]. The time-domain solutions have been obtained by inverse Laplace transforms. Analytical solutions of water hammer equations by consideration of an unsteady state friction term are a difficult task [15]. The time-domain solution for transient laminar pipe flow dependent on the dimensionless water hammer number *Wh*, defined below Eq. (4), has been recently developed by Urbanowicz et al. [30]. Exact formulas for pressure (pressure head), flow velocity and wall shear stress have been applied for the case of instantaneous valve closure in a reservoir-horizontal pipe-valve system. In this paper we will validate pressure head solution for the transient laminar and low-Reynolds number turbulent cases in a nearly horizontal pipe. The novel analytical form for pressure head in transient laminar pipe flow is [30]

$$h(x,t)=h(x,0)+BQ_0\sum_{k=1}^{2}\left(\sum_{l=1}^{\infty}(-1)^{k+l-2}e^{\lambda_{k,l}Wh}f_{Wh-k,l}\mathrm{H}\left(T_{k,l}\frac{L}{a}\right)\right), \tag{4}$$

in which $\lambda_{k,l}=2(k+l-2)+(x/L)\cdot(-1)^{k+1}$ is index, $T_{k,l}=(a/L)t-\lambda_{k,l}$ time-index dependent function, L pipe length, $h(x,0)=h(0,0)+8WhBV_0A(x/L)$ pressure head, $B=a/(gA)$ characteristic impedance, V_0 initial average flow velocity, $Wh=(Ma_0/Re_0)(4L/D)$ water hammer number, $Ma_0=V_0/a$ initial Mach number, $Re_0=V_0D/\nu$ initial Reynolds number, $h(0,0)$ pressure head at the valve ($h=H$ for horizontal pipe), $f_{Wh\text{-}k,l}$ time-index-water hammer function, and H Heaviside step function. The time-index-water-hammer function is defined by the following expression

$$f_{Wh-k,l}=\left(2-\lambda_{k,l}Wh\right)\sqrt{\frac{T_{k,l}Wh}{\pi}}e^{-\frac{\lambda_{k,l}^2Wh}{4T_{k,l}}}+\\+\left[1+Wh\left(T_{k,l}-\lambda_{k,l}+\frac{\lambda_{k,l}^2Wh}{2}\right)\right]\mathrm{erfc}\left(\frac{\lambda_{k,l}}{2}\sqrt{\frac{Wh}{T_{k,l}}}\right). \tag{5}$$

The infinite sum in the analytical solution, Eq. (4), does not mean that many terms need to be taken into account to define properly the calculated results. The upper limit of this sum determines the number of amplitudes that will be correctly simulated. In our case study (Section 3.1), during the first four theoretical periods of the pipeline ($4T_p$; $T_p=4L/a$), the pressure head history can be properly calculated by just eight terms ($l=8$). The small number of terms taken into account does not have an impact on the fit of the simulated results, so the proposed analytical solution is free of the typical Gibbs phenomenon present in other series solutions.

Zielke's analytical unsteady friction formulation [21] has been previously validated for low Re-number turbulent pipe flow numerical solutions by Trikha [31], Bergant et al. [8] and Martins et al. [12]. An analytical solution for the transient turbulent pipe flow with consideration of unsteady skin friction is not available yet. It should be noted that semi-analytical methods for transient turbulent pipe flow including unsteady friction term have been developed by Hullender [32], and García García and Alvariño [33].

2.2 1D Method of Characteristics Water Hammer Model

The MOC transformation of Eqs. (1) and (2) produces the water-hammer compatibility equations which are valid along the characteristic lines. The compatibility equations in the finite-difference form are numerically stable unless the friction is

dominant and the computational grid is coarse and, when written for computational section i, are [1]

- along the C+ characteristic line ($\Delta x/\Delta t = a$)

$$H_{i,t} - H_{i-1,t-\Delta t} + \frac{a}{gA}\left((Q_u)_{i,t} - (Q_d)_{i-1,t-\Delta t}\right) + \frac{f\Delta x}{2gDA^2}(Q_u)_{i,t}\left|(Q_d)_{i-1,t-\Delta t}\right| = 0, \quad (6)$$

- along the C– characteristic line ($\Delta x/\Delta t = -a$)

$$H_{i,t} - H_{i+1,t-\Delta t} - \frac{a}{gA}\left((Q_d)_{i,t} - (Q_u)_{i+1,t-\Delta t}\right) - \frac{f\Delta x}{2gDA^2}(Q_d)_{i,t}\left|(Q_u)_{i+1,t-\Delta t}\right| = 0, \quad (7)$$

in which Δx is space step and Δt time step. The discharge at the upstream side of the computational section ($(Q_u)_i$) and the discharge at the downstream side of the section ($(Q_d)_i$) are identical for the pure water-hammer case where pressure remains above the liquid vapour pressure (transient liquid pipe flow). At a boundary (reservoir, valve, pump, turbine), a device-specific equation replaces one of the water-hammer compatibility equations.

2.3 3D Computational Fluid Dynamics Water Hammer Model

3D CFD water hammer is simulated numerically as a time-dependent flow of a viscous compressible liquid under isothermal conditions. Flow is governed by the conservation laws for (i) mass

$$\frac{\partial \rho}{\partial t} + \frac{\partial}{\partial x_i}(\rho u_i) = 0, \quad (8)$$

and (ii) momentum. The corresponding equations are presented in tensor form with Einstein's summation convention [34]. In the case of transient laminar flow, the momentum conservation equation is

$$\frac{\partial}{\partial t}(\rho u_i) + \frac{\partial}{\partial x_j}(\rho u_i u_j) = -\frac{\partial p}{\partial x_i} + \frac{\partial}{\partial x_j}\left[\mu\left(\frac{\partial u_i}{\partial x_j} + \frac{\partial u_j}{\partial x_i} - \frac{2}{3}\delta_{ij}\frac{\partial u_l}{\partial x_l}\right)\right], \quad (9)$$

in which u_i is flow velocity, p pressure, ρ density and μ dynamic viscosity. The Kronecker delta takes the values $\delta_{ij}=0$ for $i \neq j$ and $\delta_{ij}=1$ for $i=j$ ($i, j, l = 1, 2, 3$).

In the case of transient turbulent flow, we use the model of Reynolds-averaged unsteady Navier–Stokes equations (URANS). The momentum conservation equation in this case is

$$\frac{\partial}{\partial t}\left(\rho \bar{u}_i\right) + \frac{\partial}{\partial x_j}\left(\rho \bar{u}_i \bar{u}_j\right) = -\frac{\partial p}{\partial x_i} + \frac{\partial}{\partial x_j}\left[\mu\left(\frac{\partial \bar{u}_i}{\partial x_j} + \frac{\partial \bar{u}_j}{\partial x_i} - \frac{2}{3}\delta_{ij}\frac{\partial \bar{u}_l}{\partial x_l}\right)\right] + \frac{\partial}{\partial x_j}\left(-\rho\overline{u_i' u_i'}\right), \quad (10)$$

in which $\bar{u}_i$ is time averaged velocity and u_i' velocity fluctuations. The Reynolds stresses $-\rho\overline{u_i' u_i'}$ are modeled with an appropriate turbulence model. In the case of RANS turbulence models, we used the Boussinesq hypothesis for Reynolds stresses

$$-\rho\overline{u_i' u_i'} = \mu_t\left(\frac{\partial \bar{u}_i}{\partial x_j} + \frac{\partial \bar{u}_j}{\partial x_i}\right) - \frac{2}{3}\left(\rho k + \mu_t \frac{\partial \bar{u}_l}{\partial x_l}\right), \quad (11)$$

in which μ_t represents the turbulent viscosity and can be expressed as a function of k and ε, or k and ω. Additional turbulence transport equations can include the following quantities: turbulent kinetic energy (k), dissipation rate of turbulent kinetic energy (ε) or specific dissipation rate of turbulence (ω). As the name suggests, Transition SST model predicts laminar-turbulent transition flow regime. Details of the mathematical modelling of turbulence are given in [22,34,35].

In next two sub-sections, we present (i) the valve closure model and, (ii) the mesh model and simulation parameters, two important issues in 3D CFD water hammer modelling.

2.3.1 Valve Closure Model

The water hammer is triggered by a sudden stoppage of the steady flow in the pipe by the downstream end valve. In the numerical simulation, this can be implemented as instantaneous closure, which means that at the closure start time t_0 the outlet boundary condition is changed to a wall boundary condition. This approach is appropriate for nearly instantaneous flow stoppage ($t_c << 2L/a$) with nearly vertical pressure wave fronts. This does not correspond to the flow conditions, where the flow at the valve is continuously reduced to zero during the longer closing time t_c. Here, we constructed a function that prescribes the time dependence of the flow at the valve position. Thus, the axial velocity $v_x(t)$ varies continuously from a fixed average value V_0 to a value of zero as follows

$$v_x(t) = \begin{cases} V_0 & : \quad t < t_0 \\ V_0\left(1 + \cos\left(\pi\left(t - t_0\right)/t_c\right)\right) & : t_0 \le t \le t_0 + t_c \\ 0 & : \quad t > t_0 + t_c \end{cases}, \quad (12)$$

in which $t_0 = 0.2$ s and $t_c = 0.009$ s. Other authors have used a similar power function approach for the valve closure [36].

2.3.2 Mesh Model and Simulation

The computational area is represented by a straight round tube of length $L=37.23$ m and inner diameter $D=22.1$ mm. The domain is discretized with a hexahedral mesh with cell size $\Delta_c \approx 2$ mm, Fig. 1. The number of cells is $N_c=3788484$. Martins *et al.* in [37] suggested ≈150000 as an optimal computational mesh for a geometrically (cross-sectional area of the pipe) and hydrodynamically similar case to ours cells for the laminar regime and ≈270000 cells for the turbulent regime. Since the two numerical models are comparable, we did not perform an analysis of the grid dependence of the results.

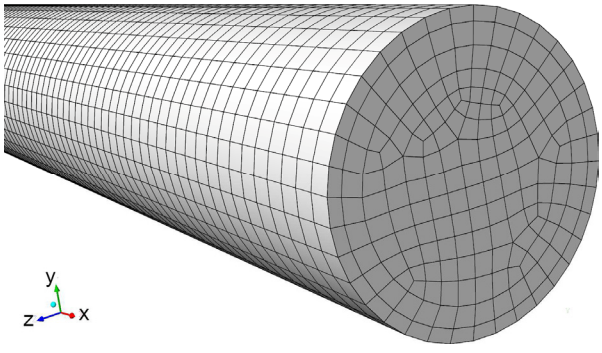

Fig. 1. Pipeline 3D computational grid

Calculations were performed with the following data from the experiment: water temperature $T_w=15.4$ °C, reference pressure $p_0=313.92$ kPa, water density at reference pressure $\rho_0 = 999.14$ kg/m³ and pressure wave speed $a=1319$ m/s. The dynamic viscosity of water at this temperature is $\mu=1.12546\times10^{-3}$ Pa·s. Because of pressure propagating waves that occur during the water hammer event, we should treat water as a compressible liquid. A compressible liquid model was used, which establishes a non-linear relationship between density and pressure under isothermal conditions. The model is derived from the simplified Tait equation of state [38]

$$\left(\frac{\rho}{\rho_0}\right)^n = \frac{1 + n\left(p - p_0\right)}{K_0}, \quad (13)$$

in which $K_0=\rho_0 a^2=1.7383\times10^9$ Pa is a bulk modulus at reference pressure and $n=7.15$ is density exponent.

For the numerical solution, we used a "pressure-based" transient type solver with either laminar or turbulent viscosity model. The turbulent flow regime was treated with the following three turbulence models: (i) Realizable k–ε model with standard wall functions, (ii) Shear–Stress Transport (SST) k–ω model and (iii) Transition SST model [22]. The boundary conditions were as follows: (i) at the inlet ($x=0$) the total pressure p_0 was prescribed, (ii) at the outlet ($x=L$) the valve closing function $v_x(t)$ was defined by Eq. (12) and (iii) at the pipe wall the velocity was $\boldsymbol{v}=0$. The initial condition for the pressure was $p=p_0$. The initial velocity values in the laminar regime were prescribed as $\boldsymbol{v}=(2V_0\,[1-4r^2/D^2],\,0)$ and in the turbulent regime as $\boldsymbol{v}=(V_0,\,0)$; r is pipe radius.

In the solver, the SIMPLE method was selected for velocity–pressure coupling. Spatial discretization was: (i) "least squares cell based" for gradient, (ii) "second order" for pressure and (iii) "second order upwind" for density, velocity and turbulent quantities. The "first order implicit" formulation was used for the transient scheme. The under-relaxation factors were: 0.3 for pressure, 1 for density and turbulent viscosity, 0.7 for velocity and 0.8 for turbulence quantities. In the model, we selected two pipeline sections where we saved the pressure value in each time step, namely at the midpoint of the pipe at $x=18.615$ m (index mp in the graphs) and at the downstream end valve at $x=37.23$ m (index v in graphs). The numerical simulation of the water hammer event took place in three steps:

(i) First, a calculation was made for steady-state conditions to develop a steady-state pipe flow velocity profile.

(ii) A switch to transient calculation mode was made with a time step $\Delta t=10^{-3}$ s for a duration of $t=1$ s.

(iii) This was followed by resetting the time to zero, turning on the pressure output at the observed locations and calculating until time $t_0=0.196$ s, when the time step was reduced to $\Delta t=10^{-5}$ s. At time $t=t_0$, the valve started to close. At time $t=t_0+t_c$, the valve was completely closed.

After the valve was closed, the calculation took another 0.4 s, which means that three full pressure fluctuations between the maximum and minimum values could be observed during this time. During this time period, the water flow was four times in the positive direction and three times in the negative direction. Such a small-time step was necessary, since the pressure rise in rapid downstream-end valve closure event is a very fast phenomenon.

2.4 Experimental Pipeline Apparatus

A versatile pipeline apparatus for investigating water hammer and column separation events was constructed at the University of Adelaide, Australia [39]. The apparatus comprises a straight 37.23 m ($U_x=\pm0.01$ m) long sloping copper pipe of 22.1 mm ($U_x=\pm0.1$ mm) internal diameter and of 1.63 mm ($U_x=\pm0.05$ mm) wall thickness, see Fig. 2. The uncertainty in the measurement U_x is expressed as a root-sum-square combination of bias and precision error [40]. A water hammer event in the pipeline was induced by rapidly closing the downstream-end ball valve. The reference [39] describes the experimental pipeline apparatus in detail.

3 RESULTS AND DISCUSSION

The results of calculation with 1D analytical and numerical MOC models, and 3D numerical model (3D CFD) are validated against the results of measurements with the Adelaide pipeline apparatus (Fig. 2). We compare the computational and experimental results for the rapid closing of the valve installed at the downstream end of the pipe for two typical cases of water hammer with initial flow velocities $V_0=\{0.1;0.3\}$ m/s (initial laminar ($Re_0=1960$) and turbulent pipe flow with low Reynolds number ($Re_0=5880$), respectively) [8]. The static head in the upstream end pressurized tank $H_{T,2}=32$ m is the same for both cases. The measured wave speed of the propagation of the first steep pressure head rise is $a=1319$ m/s. The pressure head wave speed is slightly decreasing during the transient event because the liquid has an extra inertia due to the velocity distribution, which is related to the momentum correction factor [41]. The results are compared at the valve (H_v) and at the midpoint of the pipeline (H_{mp}) (Fig. 2). The goal of the analysis is the validation of the two 1D models by consideration of quasi-2D frozen-viscosity convolutional model of unsteady wall friction, and further to extract the differences in the way of treating the transient flow according to the 1D and 3D methods.

3.1 Comparison of 1D Analytical and Experimental Results

1D analytical calculations were performed for instantaneous valve closure. The results for the run with initial flow velocity $V_0=0.1$ m/s are compared in Figs. 3a and b. The computational results obtained with the 1D analytical model (Eqs. (4) and (5)) developed for transient laminar pipe flow [30] agree well with the measured results in terms of attenuation, shape and timing of the pressure pulses. The maximum analytically calculated bulk head at the valve $H_{v\text{–}max\text{–}A}=45.7$ m differs for 1 % from the measured one $H_{v\text{–}max\text{–}E}=45.8$ m. The head trace at the midpoint has been selected for the assessment of the attenuation rate over the first four positive bulk pressure head pulses (time span of $12L/a$). The percentage of the pressure head drop $\Delta h_{mp1\text{–}4}$ is calculated by the following equation

$$\Delta h_{mp1-4}=\frac{h_{mp1}-h_{mp4}}{h_{mp1}}\times100, \tag{14}$$

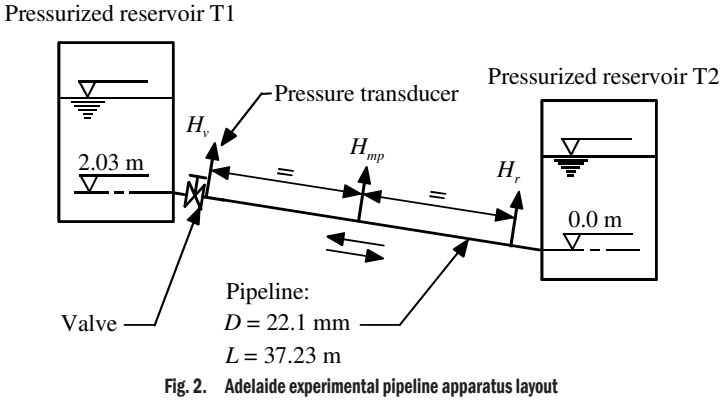

Fig. 2. Adelaide experimental pipeline apparatus layout

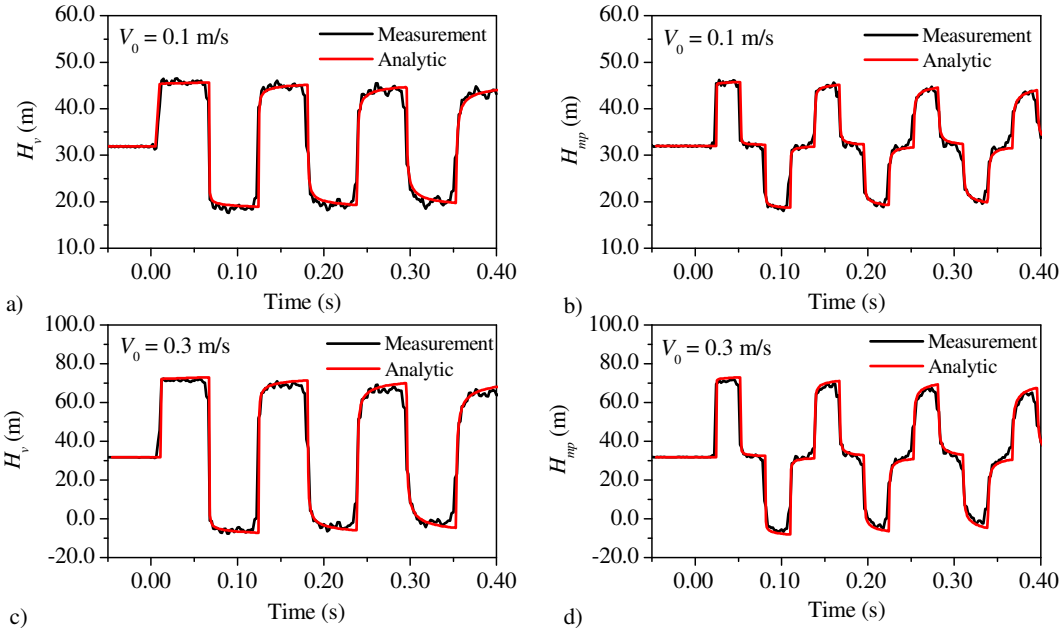

Fig. 3. Comparison of measured and 1D analytical computed head histories for laminar (Re_0 = 1960) and for turbulent pipe flow case (Re_0 = 5880); a) and c) at the valve; b) and d) at the midpoint

in which h_{mpi} is pressure head at the midpoint of the pipeline at elevation of 1.02 m (i=1,2,3,4), see Fig. 2. The calculated percentage of the pressure head $\Delta h_{mp1\text{–}4\text{–}A}$=3.8 % is slightly lower than measured one $\Delta h_{mp1\text{–}4\text{–}E}$=5.4 % (1.6 % difference).

The actual effective valve closure time is about 0.004 s, well below the wave reflection time $2L/a$=2·37.23/1319=0.0565 s. In our case the assumption of the instantaneous valve closure is acceptable as can be seen from the comparison between the measured first pressure head rise and the theoretical one in Fig. 3a.

The results for the test with initial pipe flow velocity V_0=0.3 m/s are compared in Figs. 3c and d. The unsteady friction part based on the transient laminar flow does contribute to additional energy loss for the low Reynolds number turbulent flow (Re_0<10⁴) [31]. The maximum analytically calculated bulk head at the valve $H_{v\text{–}max\text{–}A}$=73.0 m is slightly higher than the experimentally predicted head $H_{v\text{–}max\text{–}E}$=71.9 m (1.7 % difference). The calculated percentage of the pressure head drop over the observed time span $\Delta h_{mp1\text{–}4\text{–}A}$=7.5 % is slightly lower than measured one $\Delta h_{mp1\text{–}4\text{–}E}$=9.8 % (2.3 % difference). The magnitude of the deviations between calculated and measured results for turbulent flow with low Reynolds number (Figs. 3c and d) is of the same order as the one for laminar flow case (Figs. 3a and b) Finally, it should be noted that in pipeline engineering practice, the acceptable difference bewteen the calculated and measured results is 5 % for the maximum water hammer head and 10 % for the estimated friction factor.

3.2 Comparison of 1D MOC Numerical and Experimental Results

1D MOC calculations were performed for actual valve closing time t_c=0.009 s and the number of pipe sections in numerical model N=16. The results for the laminar flow case are compared against the measured results in Figs. 4a and b. The computational results obtained with the frozen-viscosity convolutional model of unsteady friction [21] agree well with the measurement results in terms of attenuation, shape and timing of the pressure pulses. The maximum MOC calculated bulk head at the valve $H_{v\text{–}max\text{–}MOC}$=45.8 m matches the measured head $H_{v\text{–}max\text{–}E}$=45.8 m. There is a slight difference between the calculated $\Delta h_{mp1\text{–}4\text{–}MOC}$=4.3 % and the measured percentage of the pressure head drop at the midpoint of the pipeline $\Delta h_{mp1\text{–}4\text{–}E}$=5.4 % (1.1 % difference). The degree of discrepancies between the 1D MOC and the 1D analytically calculated results when compared to the measured results is small. There are slight differences between the shape and timing of the pressure histories (compare Figs. 3a and b, and Figs. 4a and b).

The results for the test with initial pipe flow velocity V_0=0.3 m/s are compared in Figs. 4c and d. The maximum MOC calculated bulk head at the valve $H_{v\text{–}max\text{–}MOC}$=73.1 m is slightly higher than the measured head $H_{v\text{–}max\text{–}E}$=71.9 m (1.7 % difference). There is an excellent match between the calculated percentage of the pressure head drop $\Delta h_{mp1\text{–}4\text{–}MOC}$=9.9 % and the measured one $\Delta h_{mp1\text{–}4\text{–}E}$=9.8 %. The inclusion of weights for past velocity changes developed in the frozen-viscosity convolutional model for transient laminar pipe flow [21] contributes to additional energy loss for transient turbulent flow with low Reynolds number (Re_0<10⁴) [31]. The magnitude of the deviations between calculated and measured results for turbulent flow with low Reynolds number (Figs. 4c and d) is similar to that for laminar flow case (Figs. 4a and b).

3.3 Comparison of 3D CFD Numerical and Experimental Results

Comparisons of 3D numerical and experimental results for transient laminar and low Reynolds number turbulent flow cases are presented in this section.

3.3.1 Laminar Flow Case

First, we carried out a numerical simulation of water hammer for the case of laminar pipe flow at initial Reynolds number Re_0=1960. The average velocity of the steady water flow in the pipe was V_0=0.1 m/s. The parallel calculation took 5.67 days on 23 cores of a Supermicro workstation with four AMD Opteron® 8439 SE processors at a frequency of 2.8 GHz. It should be noted that the calculation with the 1D models only takes a few minutes.

Figure 5 compares head histories at the valve and at the midpoint. We may see a good agreement between experiment and numerical calculation. The maximum numerically predicted head at the valve $H_{v\text{–}max\text{–}CFDlam}$=45.2 m is slightly lower than the experimentally predicted one $H_{v\text{–}max\text{–}E}$=45.8 m (1.3 % difference). The calculated

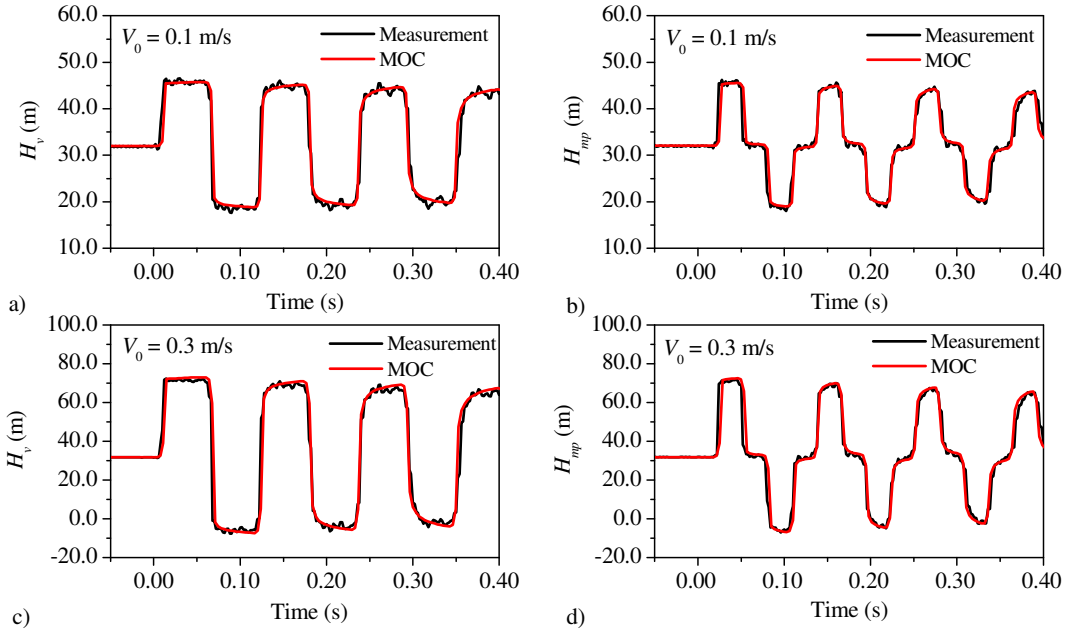

Fig. 4. Comparison of measured and 1D MOC computed head histories for laminar (Re_0 = 1960) and for turbulent pipe flow case (Re_0 = 5880): a), c) at the valve; b), d) at the midpoint

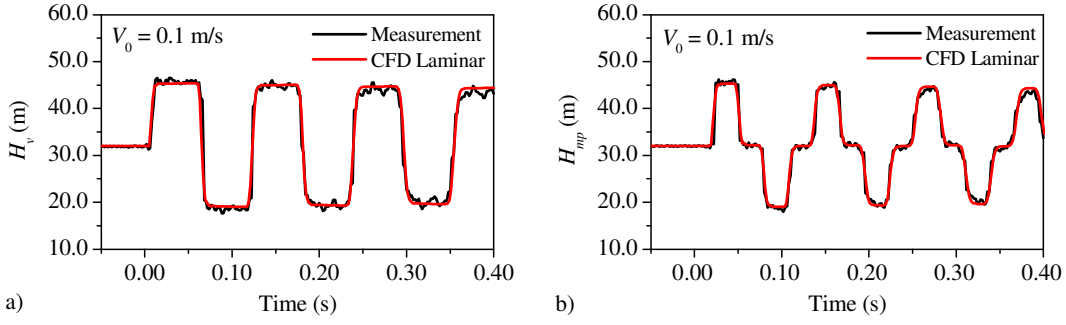

Fig. 5. Comparison of measured and computed 3D CFD head histories for laminar pipe flow case (Re_0 = 1960): a) at the valve; b) at the midpoint

percentage of the pressure head drop over the observed time span $\Delta h_{mp1\text{–}4\text{–}CFDlam}$=2.0 % is lower than the measured one $\Delta h_{mp1\text{–}4\text{–}E$=5.4 % (3.4 % difference).

The 3D CFD compressible liquid model, which establishes a non-linear relationship between density and pressure under isothermal conditions, accurately predicts the water hammer wave mechanics. The head wave history is repeated periodically with a frequency of 8.7 Hz, only the amplitude of the head rise decreases and attenuates during the transient event [8].

It should be pointed out that the damping time of the pressure fluctuation depends on the length of the pipe L at an assumed constant pipe diameter D; the unsteady friction part against the quasi-steady state friction part is decreasing as the pipe length is increasing. In case of unsteady friction dominated pipe flow situations for dimensionless quantities of L/D, quasi-steady friction factor f_{q0}, Ma_0 and Re_0 one can calculate the steady part ($f_{q0}Ma_0L/(2D)$) and the unsteady part ($(2LMa_0/(DRe_0))^{0.5}$) of the friction damping coefficient. For our laminar flow case (f_{q0}=0.035) are 0.002 and 0.011, respectively, see details in Duan et al. [42].

3.3.2 Low-Reynolds Number Turbulent Flow Case

3D CFD numerical simulation of water hammer for the case of turbulent flow at Re_0=5880 was carried out next. The average velocity of the initial pipe flow velocity was V_0=0.3 m/s. The following three commonly used turbulence models were selected [22,34,35]: (i) the two-equation k–ε and (ii) k–ω models, and (iii) the four-equation Transition SST model. Parallel calculations on the same workstation as for laminar flow case took: 6.86 days for the k–ε model, 3.71 days for the k–ω model, and 5.53 days for the Transition SST model.

Figure 6 compares head histories at the valve and at midpoint for all three turbulence models. Even in this case, the agreement between experiment and numerical calculations is reasonable. The maximum 3D CFD calculated bulk head at the valve $H_{v\text{–}max\text{–}CFDturb}$={turbulence model k–ε: 71.5 m; k–ω: 72.6 m; Transition SST: 71.7 m} agree well with the experimentally predicted head $H_{v\text{–}max\text{–}E}$=71.9 m {difference for k–ε: 0.6 %; k–ω: 1.0 %; Transition SST: 0.3 %}. The calculated percentage of the pressure head drop for the three turbulence models $\Delta h_{mp1\text{–}4\text{–}CFDturb}$={$k$–$\varepsilon$: 4.1 %; k–ω: 5.8 %; Transition SST: 5.1 %} is lower than the measured one $\Delta h_{mp1\text{-}4\text{-}E}$ = 9.8% {difference for k–ε: 5.7 %; k–ω: 4 %; Transition SST: 4.7 %}. The Transition SST model approximates the experiment slightly better (Figs. 6e and f) than the two-equation models (Figs. 6a to d). In the first period, the calculated head differs very little from the measured one, and in the following periods the discrepancy slowly grows. The amplitude of the pressure rise does not decrease as fast as in the experiment, and the frequency of the pressure head fluctuation also decreases compared to the measured values. We may conclude that small discrepancies occur

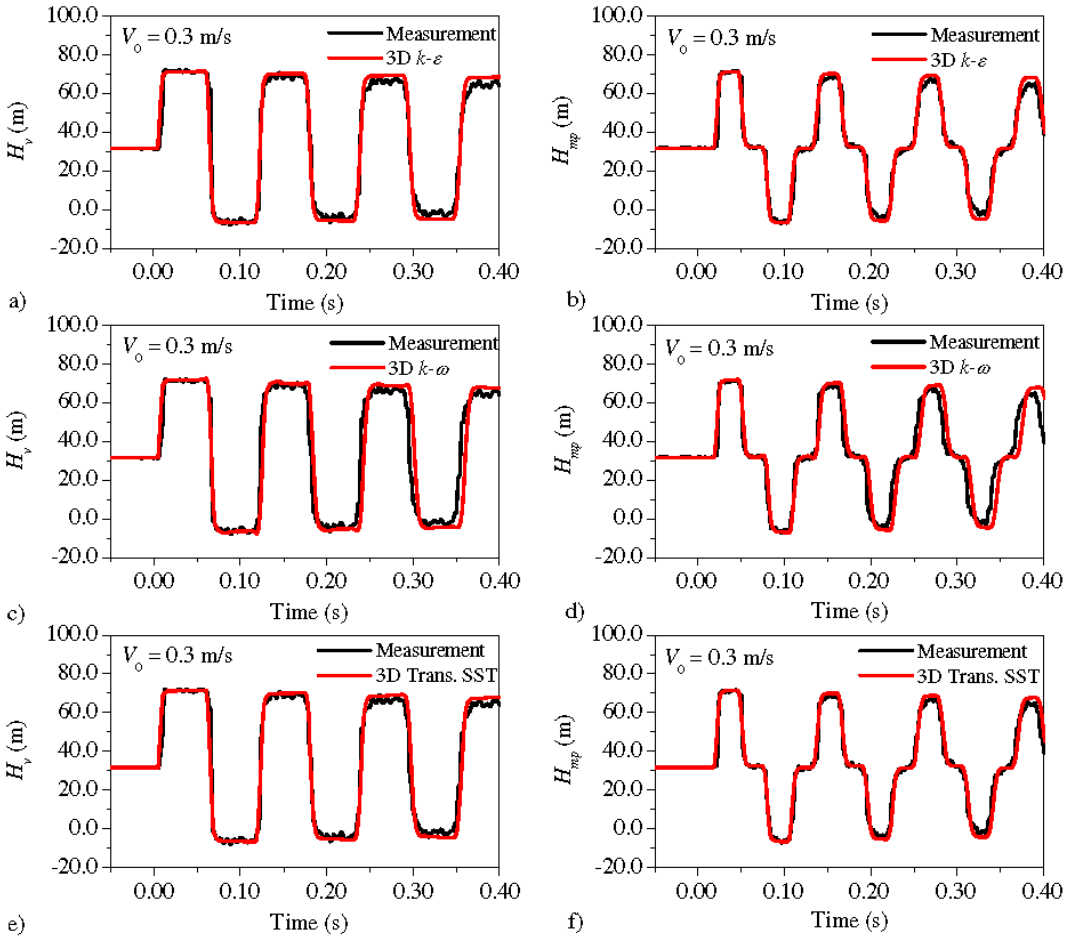

Fig. 6. Comparison of measured and computed 3D CFD head histories for turbulent pipe flow case (Re_0 = 5880): a), c), e) at the valve, and b), d), f) at the midpoint

because the *Re* number is very low; therefore, there is no turbulence model, which would have a distinct advantage.

4 CONCLUSIONS

It has been shown that both 1D analytical and 1D MOC models with consideration of laminar flow based unsteady state friction term [21] can be successfully used for low Reynolds number turbulent water hammer ($Re_0 < 10^4$). The frozen viscosity convolutional model captures the multidimensional shape of the flow velocity profile, which is represented as an average velocity in the 1D model. The multi-dimensional CFD represents a very effective and accurate tool for the analysis of flow and pressure conditions in real engineering problems which was confirmed by 3D CFD simulation of the water hammer. The 3D CFD numerical model can be further extended with two-way interaction between liquid and solid (direct coupling). High pressure loads cause high pipe-wall stress and thus elastic deformation of the pipeline, which causes a reverse change in the flow. This would give us a tool that provides a precise insight into 3D pipe flow conditions. The analytical 1D model is an excellent tool for the verification studies of numerical 1D and 3D models. The results of calculations based on the two 1D and 3D numerical models agree well with the results of the measurements obtained in a simple pipeline apparatus. Quantitative comparison analysis yields up to 2 % difference in maximum head at the valve and up to 5 % relative difference in pressure head drop at the midpoint of the pipeline monitored over the first four positive pressure pulses. Naturally, 1D models are computationally less intensive compared to a 3D CFD model. Further research is sought in theoretical (analytical solution for turbulent water hammer) and experimental investigations of high Reynolds number water hammer ($Re_0 > 10^5$), and in the future, in direct numerical simulations of water hammer events [27].

References

[1] Wylie, E.B., Streeter, V.L. *Fluid Transients in Systems*. Prentice Hall (1993) Englewood Cliffs.

[2] Chaudhry, M.H. *Applied Hydraulic Transients*. Springer (2014) New York, **DOI:10.1007/978-1-4614-8538-4**.

[3] Giljen, Z., Nedeljković, M., Cheng, Y. The influence of pump-turbine specific speed on hydraulic transient processes. *Stroj vestn-J Mech E* 70 231-246 (2024) **DOI:10.5545/sv-jme.2023.776**.

[4] Jung, B.S., Karney, B.W. Pressure surge control strategies revised. *AWWA Wat Sci* 2 e1169 (2020) **DOI:10.1002/aws.1169**.

[5] Li, H., Xu, B., Arzaghi, E., Abbassi, R., Chen, D., Aggidis, G.A., Zhang, J., Patelli, E. Transient safety assessment and risk mitigation of a hydroelectric generation system. *Energy* 196 117135 (2020) **DOI:10.1016/j.energy.2020.117135**.

[6] Kubrak, M. Modeling of closing functions for gate valves fitted with V-ports. *J Pipel Syst Eng Pract* 15 04024023 (2024) **DOI:10.061/JPSEA2.PSENG-1588**.

[7] Brunone, B., Golia, U.M., Greco, M. Effects of two-dimensionality on pipe transients modelling. *J Hydraul Eng* 121 906-912 (1995) **DOI:10.1061/(ASCE)0733-429(1995)121:12(906)**.

[8] Bergant, A., Simpson, A.R., Vítkovský, J. Developments in unsteady pipe flow friction modelling. *J Hydraul Res* 39 249-257 (2001) **DOI:10.1080/00221680109499828**.

[9] Pezzinga, G. Evaluation of unsteady flow resistances by quasi-2D or 1D models. *J Hydraul Eng* 126 778-785 (2000) **DOI:10.1061/(ASCE)0733-9429(2000)126:10(778)**.

[10] Riedelmeier, S., Becker, S., Schlücker, E. Damping of water hammer oscillations - comparisons of 3D CFD and 1D calculations using two selected models for

pipe friction. *PAMM Proc Appl Math Mech* 14 705-706 (2014) **DOI:10.1002/pamm.201410335**.
[11] Mandair, S., Magnan, R., Morissette, J.F., Karney, B. Energy-based evaluation of 1D unsteady friction models for classic laminar water hammer with comparison to CFD. *J Hydraul Eng* 146 04019072 (2020) **DOI:10.1061/(ASCE)HY.1943-7900.0001697**.
[12] Martins, S.C., Covas, D.I.C., Capponi, C., Meniconi, S., Brunone, B. Unified approach for damping rate to transient laminar flow: experiments, computational fluid dynamics, and one dimensional, and global models. *J Fluid Eng-T ASME* 146 021306 (2024) **DOI:10.1115/1.4063697**.
[13] Plouraboué, F. Review on water-hammer waves mechanical and theoretical foundations. *Eur J Mech B-Fluids* 108 237-271 (2024) **DOI:10.1016/j.euromechflu. 2024.08.001**.
[14] Kumar, M.R.A., Pu, J.H., Hanmaiahgari, P.R., Lambert, M.F. Insights into CFD modelling of water hammer. *Water* 15 3988 (2023) **DOI:10.3990/w15223988**.
[15] Urbanowicz, K., Jing, H., Bergant, A., Stosiak, M., Lubecki, M. Progress in analytical modeling of water hammer. *J Fluids Eng-T ASME* 145 081203 (2023) **DOI:10.1115/1.4062290**.
[16] Neyestanaki, M.K., Dunca, G., Jonsson, P., Cervantes, M.J. A comparison of different methods for water hammer valve closure with CFD. *Water* 15 1510 (2023) **DOI:10.3990/w15081510**.
[17] Zhang, X. Transient flow characteristics of a pressure differential valve with different valve spool damping orifice structures. *Stroj vestn-J Mech E* 70 141-158 (2024) **DOI:10.5545/sv-jme.2023.691**.
[18] Saemi, S., Raisee, M., Cervantes, M.J., Nourbakhsh, A. Computation of two- and three-dimensional water hammer flows. *J Hydraul Res* 57 386-404 (2019) **DOI:10.1080/00221686.2018.1459892**.
[19] Cao, Y., Zhou, L., Qu, C., Fang, H., Liu, D. 3D CFD simulation and analysis of transient flow in a water pipeline. *AQUA - Water Infrastr Ecosyst Soc* 71 751-767 (2022) **DOI:10.2166/aqua.2022.023**.
[20] Wang, C., Nilsson, H., Yang, J., Petit, O. 1D-3D coupling for hydraulic system transient simulations. *Comput Phys Commun* 210 (2017) **DOI:10.1016/j.cpc.2016.09.007**.
[21] Zielke, W. Frequency-dependent friction in transient pipe flow. *J Basic Eng-T ASME* 90 109-115 (1968) **DOI:10.1115/1.3605049**.
[22] ANSYS® *Academic Research CFD, Release 18.2*. Ansys (2019) Canonsburg.
[23] Vardy, A.E., Brown, J.M.B., He, S., Ariyarante, C., Gorji, S. Applicability of frozen-viscosity models of unsteady wall shear stress. *J Hydraul Eng* 141 0401064 (2015) **DOI:10.1061/(ASCE)HY.1943-7900.0000930**.
[24] Urbanowicz, K. Fast and accurate modelling of frictional transient pipe flow. *J Appl Math Mech* 98 802-823 (2018) **DOI:10.1002/zamm.201600246**.
[25] Vardy, A.E., Brown, J.M.B. Transient turbulent friction in smooth pipe flows. *J Sound Vib* 259 1011-1036 (2003) **DOI:10.1016/jsvi.2002.5160**.
[26] Vardy, A.E., Brown, J.M.B. Transient turbulent friction in fully-rough pipes flow. *J Sound Vib* 270 233-257 (2004) **DOI:10.1016/S0022-460X(03)00492-9**.
[27] Guerrero, B., Lambert, M.F., Chin, R.C. Extension of the 1D unsteady model for rapidly accelerating and decelerating turbulent pipe flows. *J Hydraul Eng* 148 04022014 (2022) **DOI:10.1061/(ASCE)HY.1943-7900.0001998**.
[28] Meniconi, S., Duan, H.F., Brunone, B., Ghidaoui, M.S., Lee, P.J., Ferrante, M. Further developments in rapidly decelerating turbulent flow modelling. *J Hydraul Eng* 140 04014028 (2014) **DOI:10.1061/(ASCE)HY.1943-7900.0000880**.
[29] Rich, G.R. Water hammer analysis by the Laplace-Mellin transformation. *J Fluid Eng-T ASME* 67 361-376 (1945) **DOI:10.1115/1.4018265**.
[30] Urbanowicz, K., Bergant, A., Stosiak, M., Karpenko, M., Bogdevičius, M. Developments in analytical wall shear stress modelling for water hammer phenomena. *J Sound Vib* 562 117848 (2023) **DOI:10.1016/j.jsv.2023.117848**.
[31] Trikha, A.K. An efficient method for simulating frequency-dependent friction in transient liquid flow. *J Fluid Eng-T ASME* 97 97-105 (1975) **DOI:10.1115/1.3447224**.
[32] Hullender, D.A. Water hammer peak pressures and decay rates of transients in smooth lines with turbulent flow. *J Fluid Eng-T ASME* 140 061204 (2018) **DOI:10.1115/1.4039120**.
[33] García García, F.J., Alvariño, P.F. On an analytic solution for general unsteady/transient turbulent pipe flow and starting turbulent flow. *Eur J Mech B-Fluids* 74 200-210 (2019) **DOI:10.1016/j.euromechflu.2018.11.014**.
[34] Tucker, P.G. *Advanced Computational Fluid and Aerodynamics*. Cambridge University Press (2016) New York, **DOI:10.1017/CBO9781139872010**.
[35] Wilcox, D.C. *Turbulence Modeling for CFD*. DCW Industries (2010) La Cañada.
[36] Martins, N.M.C., Wahba, E.M. On the hierarchy of models for pipe transients: From quasi-two-dimensional water hammer models to full three-dimensional computational fluid dynamics models. *J Press Vess-T ASME* 144 021402 (2022) **DOI:10.1115/1.4051930**.
[37] Martins, N.M.C., Carriço, N.J.G., Ramos, H.M., Covas, D.I.C. Velocity-distribution in pressurized pipe flow using CFD: Accuracy and mesh analysis. *Comput Fluids* 105 218-230 (2014) **DOI:10.1016/j.compfluid.2014.09.031**.
[38] Tait, P.G. *Report on Some of the Physical Properties of Fresh Water and of Sea Water*. Challenger Expedition, Johnson Reprint Corporation (1965) New York.
[39] Bergant, A., Simpson, *A.R. Water Hammer and Column Separation Measurements in an Experimental Apparatus*. Research Report no. R128, Department of Civil and Environmental Engineering, University of Adelaide (1995) Adelaide.
[40] Coleman, H.W., Steele, W.G. *Experimentation and Uncertainty Analysis for Engineers*. John Wiley and Sons (1989) New York.
[41] Bergant, A., Karadžić, U., Vítkovský, J., Vušanović, I., Simpson, A.R. A discrete gas-cavity model that considers the frictional effects of unsteady pipe flow. *Stroj vestn-J Mech E* 51 692-710 (2005).
[42] Duan, H.-F., Ghidaoui, M.S., Lee, P.J., Tung, Y.K. Relevance of unsteady friction to pipe size and length in pipe fluid transients. *J Hydraul Eng* 138 154-166 (2012) **DOI:10.1061/(ASCE)HY.1943-7900.0000497**.

Acknowledgements *Anton Bergant gratefully acknowledges the support of the Slovenian Research and Innovation Agency (ARIS) conducted through the research programme P2-0162. Kamil Urbanowicz declares that his contribution is financially supported by the Minister of Science under the 'Regional Initiative of Excellence' (RID) programme. In addition, this paper has been written to mark the 30th anniversary of the Slovenian Association of Hydraulic Research (SDHR).*

Received: 2024-10-01, revised: 2025-05-12, accepted: 2025-05-27 *as Original Scientific Paper*

Data availability *Data supporting the findings of this study are available from the corresponding author upon reasonable request.*

Authors Contributions *Anton Bergant: Conceptualization, Metodology, Computational Analysis, Measurements, Validation, Writing – Original Draft, Writing – Review and Editing, Supervision; Zlatko Rek: Conceptualization, Metodology, Computational Analysis, Validation, Writing – Original Draft, Writing – Review and Editing; Kamil Urbanowicz: Conceptualization, Metodology, Computational Analysis, Validation, Writing – Original Draft, Writing – Review and Editing.*

Analitične, numerične 1D in 3D raziskave vodnega udara v enostavnem preizkusnem cevovodu

Povzetek *Prispevek obravnava analitično in numerično simulacijo vodnega udara v sistemu rezervoar-cevovod-ventil (RCV). Razvita je bila analitična rešitev enačb vodnega udara z nestalnim členom stenskega trenja za prehodni laminarni tok v RCV sistemu. Za simulacijo poljubnega pretočnega stanja je bilo razvitih več 1D numeričnih metod. Fizikalno zasnovana metoda karakteristik se je izkazala za računsko učinkovito in prikladno za obravnavanje kompleksnih robnih pogojev. Natančnost 1D numeričnega modela se poveča z vpeljavo členov, ki zajemajo vpliv večrazsežnega prostora (primer nestalnega stenskega trenja). 3D model neposredno napoveduje te vplive in predstavlja odlično orodje za raziskovanje večrazsežnih lastnosti tekočin (numerični laboratorij). Rezultati izračunov, ki temeljijo na 1D in 3D numeričnih modelih, se dobro ujemajo z rezultati meritev, ob upoštevanju ustrezne napovedi in modeliranja vplivnih fizikalnih količin v stanjih laminarnega in turbulentnega vodnega udara z nizkim Reynoldsovim številom. Kvantitativna primerjalna analiza pokaže do 2 % razliko v maksimalni tlačni višini pri ventilu in do 5 % relativno razliko v padcu tlačne višine na sredini cevovoda, ki se spremlja v prvih štirih tlačnih pulzih.*

Ključne besede *cevovod, vodni udar, analitična rešitev, metoda karakteristik, računalniška dinamika tekočin, nestalno stensko trenje*